Substantial Fatigue Similarity of a New Small-Scale Test Rig to Actual Wheel-Rail System

Meysam Naeimi, Zili Li, Roumen Petrov, Rolf Dollevoet, Jilt Sietsma, Jun Wu

Abstract—The substantial similarity of fatigue mechanism in a new test rig for rolling contact fatigue (RCF) has been investigated. A new reduced-scale test rig is designed to perform controlled RCF tests in wheel-rail materials. The fatigue mechanism of the rig is evaluated in this study using a combined finite element-fatigue prediction approach. The influences of loading conditions on fatigue crack initiation have been studied. Furthermore, the effects of some artificial defects (squat-shape) on fatigue lives are examined. To simulate the vehicle-track interaction by means of the test rig, a three-dimensional finite element (FE) model is built up. The nonlinear material behaviour of the rail steel is modelled in the contact interface. The results of FE simulations are combined with the critical plane concept to determine the material points with the greatest possibility of fatigue failure. Based on the stress-strain responses, by employing of previously postulated criteria for fatigue crack initiation (plastic shakedown and ratchetting), fatigue life analysis is carried out. The results are reported for various loading conditions and different defect sizes. Afterward, the cyclic mechanism of the test rig is evaluated from the operational viewpoint. The results of fatigue life predictions are compared with the expected number of cycles of the test rig by its cyclic nature. Finally, the estimative duration of the experiments until fatigue crack initiation is roughly determined.

Keywords—Fatigue, test rig, crack initiation, life, rail, squats.

I. INTRODUCTION

ROLLING contact fatigue (RCF) is a pervasive and insidious problem on all types of railway systems [1]. During past three decades, a considerable amount of literature has been published on experimental studies of rail RCF problem. Using various testing methodologies, researchers (see e.g. [2]-[9]) utilized experimental techniques to recognize state of generation and development of RCF defects in rail material, focusing on metallurgical investigations and material microstructure.

Determination of the RCF life by full scale testing is a long and expensive process. The cost may be further increased if several variables have to be studied. In addition, great diversity in the fatigue lives of apparently identical material, even when run under closely controlled conditions, makes it necessary to test a very large number, to get a valid picture of fatigue life [10]. The application of cyclic tests in the laboratory scale is a useful method to assess the qualitative

Meysam Naeimi, Zili Li and Rolf Dollevoet are with the Section of Railway Engineering, Faculty of Civil Engineering and Geoscience, Delft University of Technology, Stevin II Lab, Stevinweg 1, 2628 CN Delft, the Netherlands (e-mail: m.naeimi@tudelft.nl).

Roumen Petrov, Jilt Sietsma and Jun Wu are with the Department of Materials Science and Engineering, Delft University of Technology. Roumen Petrov is also with Department of Materials Science and Engineering, Ghent University, Ghent, Belgium.

and quantitative influences of specific parameters on the fatigue life of material, by systematic variation of these parameters in the tests [11].

The primary assessment of fatigue initiation life in the material or its ultimate performance after crack initiation is a long-term process, even in the laboratory environment. Therefore, most of the RCF testing methods, are utilizing accelerated methodologies to expedite the experiments. A quick and relatively inexpensive way of fatigue life prediction under rolling contact conditions is addressed in [10] for roller steel bearings. Some other examples of accelerated test facilities for RCF investigations of steel bearings can be found in [12]-[15], minimizing the time of experiments to extend the number of specimens and variables.

Despite a long history of the testing facilities, due to inherent limitations of the laboratory works, the existing experimental facilities are not fully equivalent to the actual railway system. Available test rigs on wheel-rail contact studies mostly simulate the static behavior of the contact problem, while the effect of dynamic impact loading is still missing. Although extensive research has been carried out on testing approached in railway field, available methods are mostly restricted to the category of twin discs (see e.g. [16]-[19]) or roller rigs (see e.g. [20]-[22]) in which the real mechanism of rail RCF cannot be fully addressed. This is in principle because of the much difference between the loading conditions of the experimental setup and those of the actual railway. Furthermore, in these test rigs little attention has been paid to the effect of impact loading condition on RCF. In addition, no wheel-rail test rig has been found that considered the detailed-track system in the experimental setup. Moreover, the effects of high-frequency dynamics of wheel-rail contact and short-wavelength vibration of the system on rail RCF is neglected.

To overcome these limitations, a new testing methodology is designed, that adequately covers the fatigue similarity of experimental setup with that of actual railway system. The prescribed test rig minimizes the duration of fatigue experiments, while the principal analogy of the vehicle-track integration is maintained. This test rig provides the possibility of examining different variables, through the use flexible loading conditions and diverse components. A schematic view of the proposed rig is shown in Fig. 1. The wheel assembly, composing of several subassemblies representative for the primary suspension of the railway vehicle, is supported by a flatten frame system above the railway track ring (4m diameter). Multiple wheel passage on a single rail track bed is systematically provided. The rail track assembly is composed

of different subassemblies as the components of railway track structure, which is bended around a central pivot to provide a circular rail ring. The overall scale of the test rig is 1/5 relative to the actual system, while there is possibility to examine smaller wheel-rail geometries. A description of geometric parameters, material properties and operational conditions of the test rig are listed in Table I.

TABLE I
GEOMETRIC PARAMETERS, MATERIAL PROPERTIES AND OPERATIONAL CONDITIONS OF THE TEST RIG

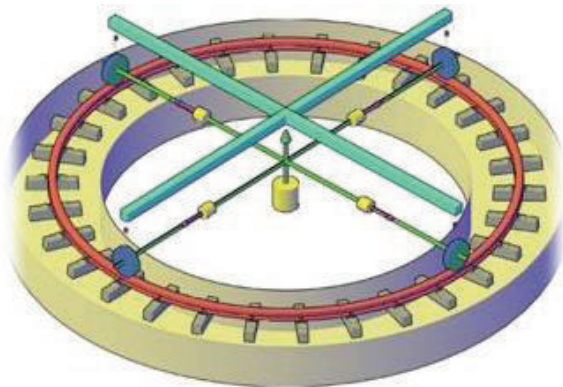| Item	Specifications
Rail	Rail: 28 mm width*32mm height (adjustable size); Rail inclination: 0 to 1:10, adjustable; Rail weight: 5 Kg/m per length; Rail ring diameter: 4 m; Rail material: adjustable (basic material: 900 A (R260));
Wheel	Wheel diameter: Ø 250 mm, (adjustable size); Wheel material: adjustable (basic material: R7T); Wheel weight: 9.4 kg,; Wheel axle diameter: 40mm, adjustable;
Sleeper	Sleeper mass: 1.6 kg, adjustable, wooden/ steel/concrete; Sleeper spacing: 140 mm, adjustable; Sleeper size: 50**50*210mm, adjustable;
Fastening	Flexible clamps with adjustable preload (toe load);
Rail pad	Railpad dimensions: 30*40mm, adjustable;
Ballast	Ballast height: 60 mm under sleepers, adjustable;
Operation and loading condition	Vertical preload on wheel: maximum 750 kg, adjustable; Traction/ braking coefficient: 0 to 0.45, adjustable; Friction coefficient: 0 to 0.6, adjustable; Rolling speed: Average: 40km/h , Maximum 60km/h. Traction/ braking coefficient: 0 to 0.45, adjustable; Friction coefficient: 0 to 0.6, adjustable;

Fig. 1 Schematic view of the new test rig (multiple wheel on single rail track)

The important fatigue properties of the new test rig are discussed in the present research. The paper first gives a brief overview of Multiaxial fatigue analysis in wheel-rail contact. The fatigue life of rail material has been estimated in the test rig model, on the basis of finite element modelling and fatigue crack prediction technique. Two fatigue initiation criteria (plastic shakedown and ratchetting), have been recognized to proceed the fatigue evaluation. Then, the results of fatigue life predictions are compared with the cyclic mechanism of the test rig to estimate the operational time of the tests to the crack initiation limit. The diagram of the overall research process is
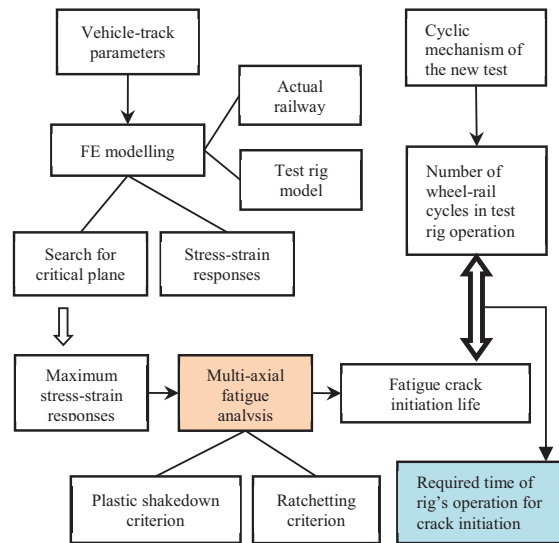
shown in Fig. 2.

Fig. 2 General procedure of the research, fatigue mechanism of the scaled test rig

II. FATIGUE ANALYSIS OF RAIL MATERIAL IN TEST RIG

Fatigue analysis is carried out to quantify the fatigue behaviour of rail materials in the new test rig. A Multiaxial fatigue criterion based on the critical plane concept is used in order to assess the fatigue crack initiation of rail material under the operational conditions of the rig. Finite element modelling (FEM) is employed as a practical technique to simulate the frictional-rolling contact behavior of wheel-rail materials and provide stress histories. Afterward, suitable fatigue criteria are exploited for fatigue life prediction of rail using the history of element stresses in the FE tool. This approach provides the opportunity of determining the crack initiation life of the rail material in the rig's environment.
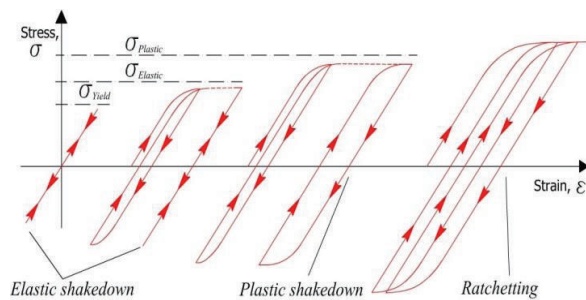

Fig. 3 Principle of material response from repeated stress cycles

A. Fatigue Crack Initiation Criteria

The stresses in materials induced by rolling contact lead to different responses, depending on the level and nature of stresses. Based on the stress-strain conditions, material response under rolling contact can be divided into three types: elastic shakedown, plastic shakedown and ratchetting (see Fig. 3). Factors that govern the type of material response are in

principle, the magnitude of the contact loads, the material hardening, the residual stress states and changes in contact conditions due to wear and plastic deformation [23], [24]. The elastic shakedown response is rare in rail material as it occurs if the contact stresses are under the yield limit. Plastic shakedown and ratchetting are two common responses of rail materials that normally cause fatigue crack initiation [25], [26].

A fatigue criterion can be employed to quantify the fatigue impact from the evaluated stresses and strains. An overview of some predictive models of fatigue crack initiation in engineering materials including rail steel is given in [27], [28]. A combination of a multiaxial fatigue criterion and a ratchetting criterion has proven to be very successful in predicting fatigue initiation in rails, see [29], [30]. In the wheel-rail rolling contact problem, the rail is subjected to a non-proportional multiaxial stress state, which results in the variation of the principal stress and maximum shear stress-strain directions during the passage of the wheel [23]. Therefore, the multiaxial fatigue criterion of Jiang-Sehitoglu [31], [32], including the non-proportional loading condition is considered in the current study, based on the critical plane approach. In addition, the well-recognized criterion of ratchetting failure in rail material proposed by Kapoor [33] is employed to predict the ratchetting life.

B. Multiaxial Fatigue Criterion

Based on [31], the multiaxial fatigue model of the current study is expressed by following equation:

$$FP_{max} = (\langle \sigma^{max} \rangle \frac{\Delta \varepsilon}{2} + J \Delta \tau \Delta \gamma)_{max} \tag{1}$$

where $\Delta \varepsilon$ is the normal strain range, σ_{max} is the maximum normal stress, $\Delta \gamma$ is the shear strain range, $\Delta \tau$ is the shear stress range, J is a material-dependent constant and $\langle \rangle$ denotes the McCauley bracket $x = (x + x)/2$. The constant J is obtained from tension/torsion tests. All the stress and strain quantities in (1) are on the critical plane, where the fatigue parameter FP is the maximum (FP_{max}). Through a tensor rotation for the stress and strain, the maximum FP and the critical plane are determined by surveying all the possible planes at a material point. The first term in (1) considers the mean stress effect. The proposed multiaxial fatigue model has the correct form to capture the synergism between the shear and normal stress components. In the current study, dominant shear crack initiation is modelled using large values of J, where $\Delta \gamma$ governs crack growth and its direction.

Based on an energy-based approach [34], [35], the relationship between fatigue parameter and crack initiation life is described by the following equation, in which the fatigue life to crack initiation has been related to the damage parameter FP_{max}.

$$FP_{max} = \frac{(\sigma'_f)^2}{E}(2N_f)^{2b} + \sigma'_f \varepsilon'_f (2N_f)^{b+c} \tag{2}$$

where N_f is the crack initiation life, corresponding to the maximum fatigue parameter FP_{max}, b, c are respectively, fatigue strength exponent and fatigue ductility exponent, σ'_f is axial fatigue strength coefficient and ε'_f is axial fatigue ductility coefficient. This equation is used in proportional and non-proportional loading of materials with cracks according to mode I [36]. Such criterion assume the influence of normal and shear stress and strain in the critical plane on fatigue life. For materials characterized by mode I cracks, the critical plane is the plane of the maximum normal strain range $\Delta \varepsilon$. However, for materials with mode II cracks, the critical plane is the plane of the maximum shear strain range $\Delta \gamma$, for which, the fatigue damage can be expressed by:

$$FP_{max} = \frac{(\tau'_f)^2}{G}(2N_f)^{2b} + \tau'_f \gamma'_f (2N_f)^{b+c} \tag{3}$$

in which G is the shear elastic modulus and τ'_f, γ'_f are shear fatigue strength and the shear fatigue ductility coefficient, respectively. Equation (2) has been employed in the current study, due to wider range of application in wheel-rail contact fatigue.

Fatigue damage is assumed to accumulate linearly. Therefore, the pertinent fatigue damage per loading cycle n can be written as:

$$\left(\frac{dD_f}{dN}\right)_n = \left(\frac{1}{N_f}\right)_n \tag{4}$$

where D_f is the fatigue damage, which is equal or smaller than 1, $\frac{dD_r}{dN}$ is the fatigue damage per cycle and N_f represents the number of loading cycles to reach the fatigue initiation limit.

C. Ratchetting Criteria

According to [33], considering a constant ratchetting rate in material, the equivalent ratchetting plastic strain per cycle n can be expressed as:

$$|d\gamma_{xz}/dN|_n = \sqrt{(\Delta \varepsilon)^2 + (\Delta \gamma / \sqrt{3})^2} \tag{5}$$

where $\Delta \varepsilon$ and $\Delta \gamma$ are the incremental ratchetting normal and shear strain per cycle on the crack plane in three-dimensional stress-strain states. The equivalent ratchetting strain is calculated on the plane with the largest shear strain accumulation. Then, the ratchetting life can be estimated by:

$$N_r = \frac{\varepsilon_c}{|d\gamma_{xz}/dN|_n} \tag{6}$$

where ε_c is the critical strain for failure by ratchetting. The ratchetting damage per load cycle n can be calculated as:

$$\left(\frac{dD_r}{dN}\right)_n - \left(\frac{1}{N_r}\right)_n \tag{7}$$

A competitive approach is proposed in the summation of total damage. The contribution to total damage summation is governed by the failure mechanism, either fatigue or ratchetting, that results in the largest damage component for the current load cycle, *n* [29]. Damage is assumed to accumulate linearly for every load cycle, as:

$$D = \sum_{n=1}^{N_f} max\left[\left(\frac{dD_f}{dN}\right)_n , \left(\frac{dD_r}{dN}\right)_n \right] \qquad (8)$$

The above formulations allow identifying the parameters that control the fatigue failure of material. It is suggested that the failure mechanisms of fatigue and ratchetting are independent and competitive, so that the life of the component is governed by the combination of fatigue damage and plastic ratchetting under rolling contact conditions [37].

D. Critical Plane Concept

The stress and strain quantities in (1) should be taken on the crack plane where the fatigue parameter has its maximum. This plane is sought by tensor rotation for the stress and strain, and the maximum FP (FP_{max}) is determined by surveying all of the possible material planes at a material point. The damage accumulation on the crack plane is the highest among all of the possible material planes, which is estimated with the stress and strain quantities calculated by finite element method. Due to the three-dimensional modelling of the rolling contact problem in this study, it is possible to obtain all six components of the stresses in the materials. The stress-based critical plane models require the evaluation of shear and normal stresses acting on the material planes. Fig. 4 gives the crack plane of material, as well as critical plane orientation and angles. The maximum value of the Von Mises stress is searched for all nodes and various plane orientations in rail material to find the probable locations of the crack initiation. The crack plane orientation is determined based on the maximum value of FP for the material point in the critical plane.
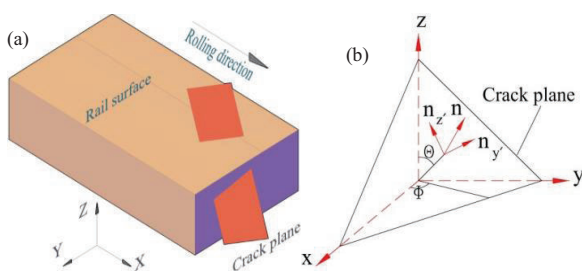

Fig. 4 (a) Crack plane of material in 3D view, (b) critical plane orientation and angles

E. Finite Element Analysis

Finite element modelling is employed to investigate the states of stresses and strains in wheel-rail material. General mechanism of the test rig is simulated using the 3D elastic–plastic FE model. Fig. 5 shows the typical FE models of the current study. In addition to the test rig model (Fig. 5 (a)); an equivalent model of actual vehicle-track interaction (Fig. 5 (b)) is also built, considering the frictional rolling contact. The FE approach is used for modelling a portion of the rail track and a single wheel component. The resilient components of the system including vehicle's primary suspension, fastening system and ballast layer are modelled with arrangement of the spring-damper elements. The wheel, rail and sleeper components are modelled with 3D solid elements. The same element type is also used for the frame component in the test rig model. In order to achieve a high accuracy of the solution with a reasonable model size, non-uniform meshing is used with finer elements in the contact surfaces, and with the finest meshing in the solution zone, see Fig. 6. The standard rail profile 54E1 with an inclination of 1:40 is used in the actual wheel-track model. The tread conicity of the wheel is set to be 1:40 as well. Thus, the wheel–rail contact occurs in the middle of the rail top.

Applying the scale factor of 1/5, the scaled geometry of the test rig model is determined. The geometric and mechanical parameters of the components in the small-scale test rig are obtained using dimensional analysis based on [38], [39]. The parameters of the two FE models are listed in Table II. Corresponding values of the actual railway model are extracted from [40].

TABLE II
THE VALUES OF PARAMETERS USED IN FE SIMULATIONS OF TWO MODELS

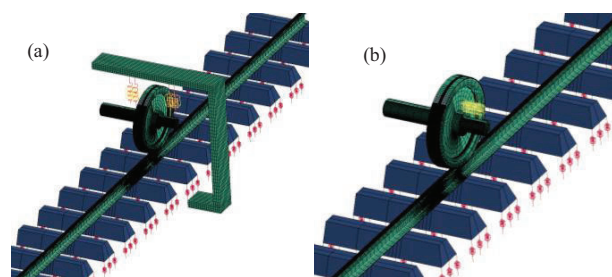| Geometries/mechanical parameters/material properties (unit)	Actual FE model	Test rig FE model
Static wheel load, P_0 (kN)	120	480
Wheel weight (kg)	900	7.2
Sleeper mass M_s (kg)	280	1.6
Stiffness of ballast, K_b (kN/m)	45000	9000
Damping of ballast, C_b (N.s/m)	32000	1280
Stiffness of rail pad, K_p (kN/m)	1300000	260000
Damping of rail pad, C_p (N.s/m)	45000	1800
Stiffness of primary suspension, K_c (kN/m)	1150	230
Damping of primary suspension, C_c (N.s/m)	2500	100
Young's modulus of wheel-rail, E_r (GP)	210	210
Poisson's ratio of wheel-rail material, v_r	0.3	0.3
Density of wheel-rail material, ρ_r (kg/m3)	7800	7800
Young's modulus of concrete, E_c (GP)	38.4	38.4
Poisson's ratio of concrete material, v_c	0.2	0.2
Density of sleeper material, ρ_c (kg/m3)	2520	2520
Rolling speed (km/h)	40	40
Friction coefficient	0.35	0.35
Traction coefficient (tangential loading)	0.15	0.15

Fig. 5 FE model of (a) the small-scale test rig, (b) actual-size vehicle–track interaction
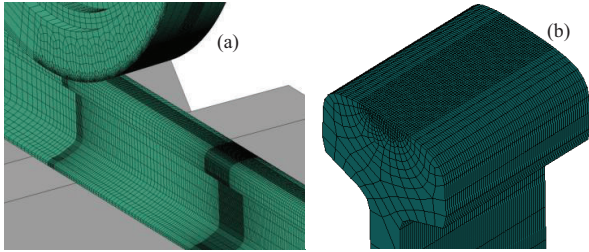
Fig. 6 (a) Adaptive meshing scheme of wheel-rail components in the FE models, (b) close view of the railhead

F. Material Model and Parameters

The linear elastic material behaviour is considered for the wheel, axle, concrete sleepers, and the steel frame (see the components in Fig. 5). Such a linear model also used for the rail elements that are far from the contact zone. The consecutive model of the rail material in contact interface are represented by the combined nonlinear isotropic and kinematic hardening model available in LS DYNA [41], which is developed by Lemaitre and Chaboche [42], [43]. It can be used for simulation of cyclic plasticity and ratchetting material response with decaying ratchetting rate [44]. The plasticity parameters of the material model used in the current study are extracted from [44]. Table III gives the material properties of the pearlitic rail steel employed in this study.

TABLE III
MATERIAL PROPERTIES OF THE PEARLITIC RAIL STEEL IN THIS STUDY

Parameter	Unit	Value	Parameter	Unit	Value
σ_y	MPa	456	$\underline{b}$	MPa	10.7
k_e	MPa	234	$\underline{c}$	GPa	6.49
E	GPa	210	γ	-	14.4
v	-	0.3	K_∞	MPa	22.8
ε_f'	%	10.3	ε_c	%	11.5
σ_f'	MPa	936	b	-	−0.089
γ_f'	%	15.45	c	-	−0.559
τ_f'	MPa	468			

III. RESULTS OF FATIGUE LIFE PREDICTION

FE simulations were carried out for the prescribed models of Fig. 5 and the time histories of stress-strain responses were acquired. The distribution of stress states at different time steps were calculated and transferred to the principal stresses within the described critical plane approach. In addition, the values of Von Mises (VM) stresses and plastic strains were extracted for the material points in the contact area. Based on the states of VM stresses, the points with the highest VM stress levels were recognized as the material points that possess the greatest risk of failure and fatigue damage. These material points were determined for the two FE models and considered as the potential locations of fatigue crack initiation (called as critical points herein after). The evolution of stress components of the critical points at different time steps of wheel passage are given in Fig. 7. As shown there, when the wheel is approaching to the recording point, the material point acquires larger quantities of stresses/strains. A reverse alteration scheme happens when the wheel is passing away

from the critical point. Furthermore, some portions of the stresses and strains are remained as the residual components after the wheel passage.
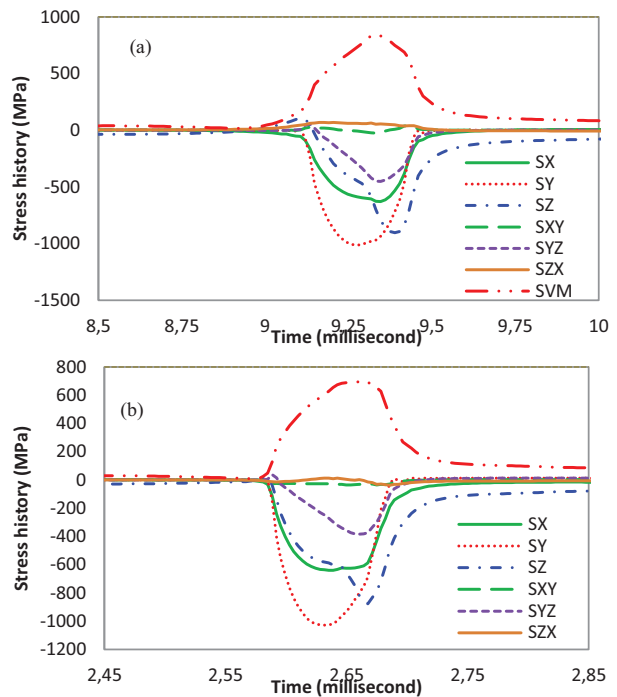

Fig. 7 Evolutions of stress components in critical point for (a) the actual railway model, (b) the test rig model
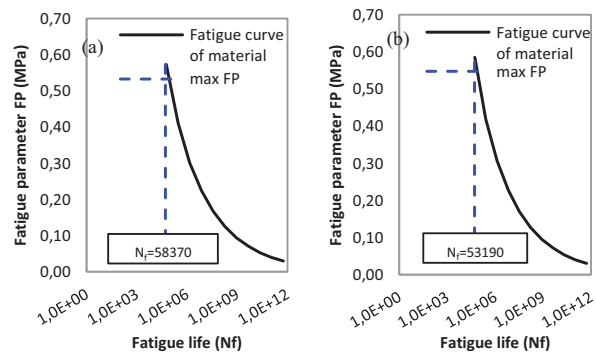

Fig. 8 Fatigue life curve of rail material at critical point for (a) the actual railway model, (b) the test rig model

After determining the stress histories of the material points, the direction of the critical plane was calculated by using the tensor rotation technique. The results of FEM and critical plane approach were used as the inputs of fatigue analysis in (1) and (2). Then, using the results of fatigue parameter (*FP*) in various load steps (during one wheel passage), the minimum number of cycles was determined as the fatigue life (N_f). Fig. 8 demonstrates the fatigue life curve of rail (at the critical point) for the FE models of the current study. The results of the test rig model were obtained for the equivalent loading condition of the actual railway; see Table II for the

parameters. These results indicate that the fatigue lives of both FE models are relatively close to each other, with around 9% difference. Indeed, when the equivalent loading conditions are employed for the both models, the fatigue life of material in the test rig model has been found to be 9% smaller than that of the actual railway.

Considering two consecutive cycles of wheel passage, the incremental ratchetting strains of material were determined for the two FE models, see Fig. 9 (a). Using (5) and (6), the number of cycles to crack initiation by ratchetting (N_r) was estimated. Fig. 9 (b) gives the ratchetting life of rail material for the both FE models. As can be seen in the figure, the rail material has nearly shown close ratchetting lives in both models with 12% difference (12% lower ratchetting life is found in the test rig model).

Comparing the number of cycles in Figs. 8 and 9, it is apparent that the crack initiation life of rail material is dominantly governed by cyclic fatigue (N_f) rather than ratchtting failure (N_r). These observations are consistent with those of the previous studies, see e.g. [25], [45]. Therefore, the values of N_f are considered as the number of cycles to fatigue crack initiation in these models. Using this, the fatigue lives of rail material are $N_f=58370$ and $N_f=53190$ for the actual model and for the test rig model respectively.
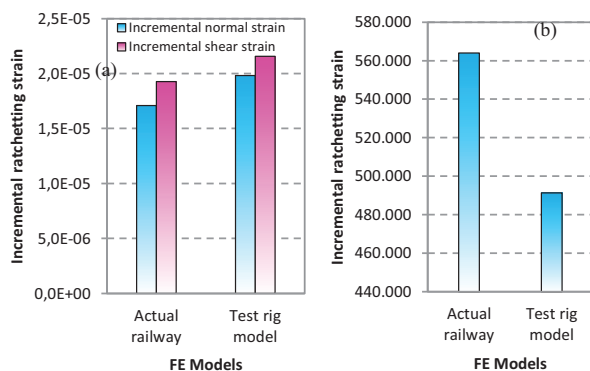

Fig. 9 (a) Incremental ratchetting strains of material in two FE models, (b) ratchetting life of material

IV. Accelerated Fatigue Sources in the Test Rig

So far, the fatigue lives of rail material were determined for the actual railway and for the test rig model. The influences of some parameters are thoroughly studied in this section, to examine the possibility of accelerated tests.

A. Effect of Wheel Preload

As shown in Table II, the static preload of the test rig model (P_0) is 480 kg, equivalent to the 120 KN wheel load of the actual railway. By employing different preload, a parametric study was carried out and the corresponding fatigue lives were determined. The load factor was defined by P/P_0, in which P_0 and P are the primary (480 kg) and the new preload of the test rig model respectively. Fig. 10 shows the variations of fatigue lives with respect to the vertical load factor. Looking at this figure, a strong relationship between the fatigue life and the

load factor can be observed. For instance, when the vertical load is increased by 50% and 100% (load factors of 1.5 and 2.0), the fatigue life of material is respectively reduced to around 51% and 23% of the primary value.
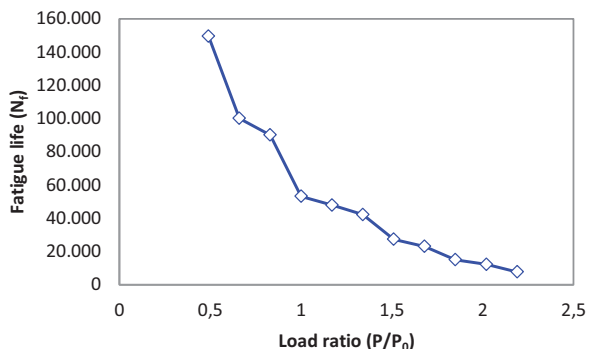

Fig. 10 Effect of wheel preload on fatigue life of rail material

B. Effect of Traction Force

A parametric study was carried out by changing the traction coefficient of the wheel-rail contact in the rolling direction. According to Table II, the primary value of the traction coefficient (μ) has been set to 0.15 for the ordinary solution in the previous sections. Here the new values of μ ranging from 0.1 to 0.5 (with eight steps) have been further examined. The influences of tangential force variation, on fatigue life in the test rig are given in Fig. 11. The results of this investigation suggest a significant reduction of the fatigue life for the models with larger traction coefficients. For instance, employing the traction coefficient of 0.45 instead of 0.15 (three times of the primary value), has leaded to around 47% reduction in fatigue life.
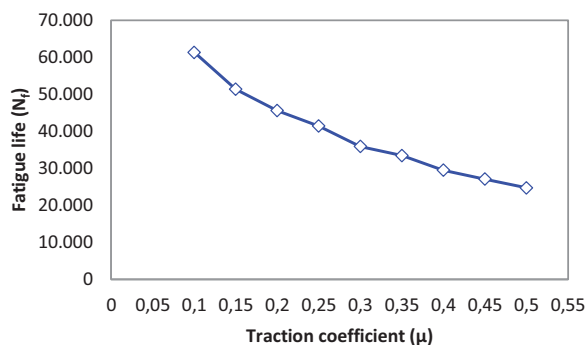

Fig. 11 Effect of tangential force on fatigue life of rail

C. Effect of Artificial Defects

Rail surface defects are an important source of wheel–rail impact and dynamic forces in railway system [46]. Among them, squats, a kind of rolling contact fatigue are generally found in the running band of the rail top and have very detrimental effects on the track [47]. In order to accelerate the fatigue experiments of material in the new test rig, it is possible to apply some artificial defects on rail top. These defects can be considered as the source of dynamic excitations

in various stages of squat development, and can exacerbate the process of material deterioration. To simulate the presence of surface defects on rail, five sample defect geometries were modelled based on the records of the measured rail profiles data. Apart from the smooth rail, the geometric models of five squats at different stages of development were simulated either in V or W shapes (see [48] for the growth mechanism of the squats). The geometric scale of 1/5 is further applied on the defect profiles to consider the scaling factor in the test rig. The vertical-longitudinal profiles of the selected defects are shown in Fig. 12 (middle of the running band). Furthermore, to derive the 3D geometry required, it is assumed that depth distribution of the squats is parabolic along the lateral direction.
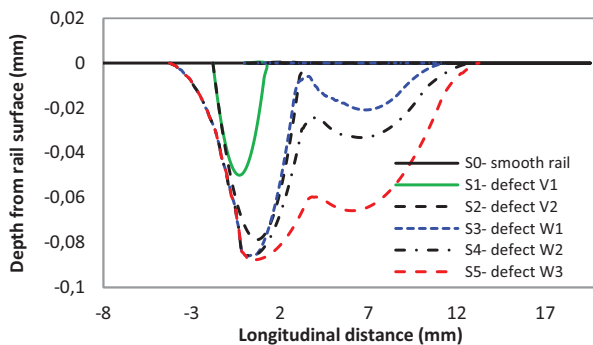

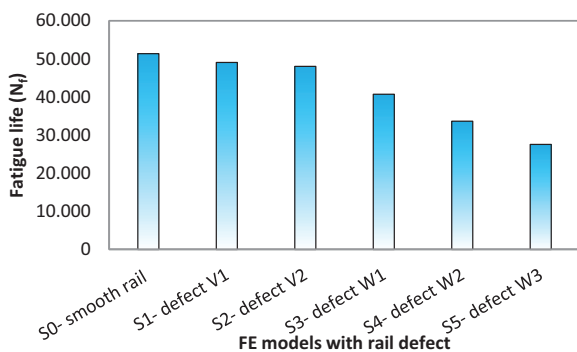Fig. 12 The profile of the simulated defects on rail surface

Fig. 13 Effect of rail surface defect on fatigue life of rail

Following the mentioned steps of fatigue analysis, the fatigue life of rail material was determined for different defect models. Fig. 13 gives the results of life estimations, by applying such defects on rail. Comparing the required number of cycles for fatigue in different scenarios, it is apparent that the crack initiation life of material is dominantly affected by the presence of the defects. As can be expected, the maximum fatigue life is recorded for the smooth rail profile. When the size of defect is increased, lower values of N_f are observed. It is also noteworthy that, the fatigue life of material is decreased with a more significant rate by the presence of W-shape defects than V-shape ones on rail surface.

V. Cyclic Nature of Wheel-Rail Contact in the Rig

Simulation of RCF problem under cyclic occurrence of wheel-rail contact is the primary goal of the new test rig. So far the fatigue life of rail material in the test rig environment has been estimated using a combined FEM-fatigue prediction approach. In this section, the cyclic nature of the rig is evaluated from the operational point of view. As described before, the test rig consists essentially of maximum four wheel components rotating on a 4m-diameter rail-track ring, see Fig. 1. The cyclic operation of the wheel on the track naturally provides the possibility of RCF experiments in materials. The wheel components are allowed to rotate in adjustable loading conditions (see Table I) driven by the electro-motors to provide a combination of rolling and sliding, similar to that experienced in the actual railway system. In the normal operational condition of the test rig, the wheels rotate at the speed of 40 km/h, but the possibility of larger speeds up to 60 km/h is also seen.

An outstanding feature of the rig concerns the high number of load cycles to which the rail is subjected during wheel running. Based on the assumptions of Table I, each wheel component can normally reach the speed of 1153.30 rev/min (rpm), for the average speed of 40 km/h. Therefore, the number of rail contact cycles will be 53.05 rev/min per one wheel on 4m-diameter rail ring. For the case of multiple wheel application with four-wheel arrangement, the number of rail contact cycles would be 212.20 rpm for the same track radius. That would be roughly the equivalent on a railway line of a continuous load of about four ICE-trains per minute (each train assumed to be consisting of 13 cars with 4 wheelsets, hence: $4 \times 13 \times 4 = 208$). Therefore if the rig continuously works, it is possible to reach more than 300000 cycles in one day (24 hours). Any stop in operation will apparently increase the duration time of the experiments and RCF initiation in rail material. Table IV demonstrates the estimative number of cycles (both in wheel and rail) for different duration periods of the experiments. The results were obtained for the arrangement of four-multiple wheel passages. Fatigue mechanism of the test rig is analysed based on the number of cycles for rail contact occurrence. The corresponding numbers of wheel cycles are merely provided for comparison.

According to Table IV, with the test rig operating up to one hour at the running speed of 40 km/h for instance, the rail surface can reach 12732 cycles of wheel-rail contact. The wheel part however, experiences 69198 numbers of cycles in one hour operation. From this table, it can be anticipated, that the manifestations of fatigue and wear that take months or even years to emerge in reality, can be achieved within a short period of time on the test rig. Furthermore, it should be noted that, reaching 50,000 cycles of loading, can be roughly considered equivalent to approximately 1 million gross tons (MGT) in the reality ($50,000 \times 20$ ton ′average axle load′ = 1MGT). This table also gives the equivalent load value of each duration time of the test rig in MGT. Looking at such data, it takes for instance around one day (24 hours) to reach 6 MGT loading over the rail in laboratory condition, a quantity that

normally takes long time for trains in the actual service.

TABLE IV
ESTIMATION OF OPERATION TIME TO REACH FATIGUE LIMIT

duration (hours)	1	6	12	24 (1day)	48 (2day)
Wheel cycles	69,198	415,186	830,373	1,660,746	3,321,491
Rail contact cycles	12,732	76,394	152,789	305,577	611,154
Equivalent tonnage (MGT)	0.25	1.53	3.06	6.11	12.22

VI. DISCUSSION

The results of fatigue life predictions can be compared with the data obtained from cyclic mechanism of the test rig. A summary of the results is presented in Fig. 14, in which the number of cycles (from the test rig operation) is correlated to the operational time of the experiments. A linear line is derived for this correlation assuming that the test rig continuously operates. Furthermore, the fatigue lives of rail material (obtained from fatigue analysis) are plotted in the figure.
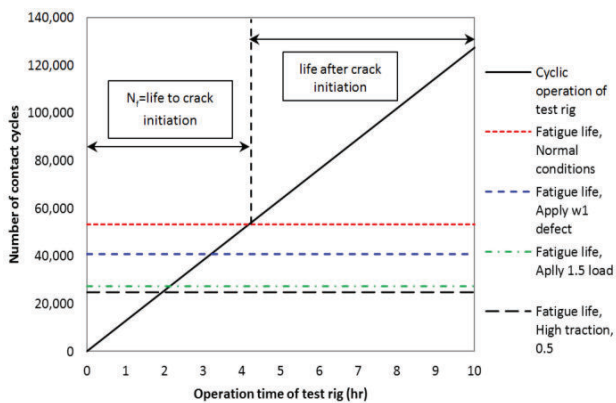

Fig. 14 Results of fatigue life predictions in rail

This figure is quite revealing in several ways. First, the crack initiation limit (fatigue life) of rail material occurs in a few hours of test rig operation. For the selected loading history and material properties of the current research for instance, it takes near 4.2 hours to experience the crack initiation limit. Second, by applying the artificial defects or by changing the loading conditions, it is possible to accelerate the fatigue initiation of material even to less period of time. Three examples of this are shown in the figure for w1 defect, load factor of 1.5 and the traction coefficient of 0.5. It is apparent from these values that the fatigue tests can be conducted with more accelerated speeds, compare to the primary value of 4.2 hour. Third, the test rig is able to be operated for the longer periods than the fatigue life limit, to simulate the fatigue growth of rail material. This period is identified in the figure with the term of "life after crack initiation". Therefore, using the prescribed fatigue mechanism of the test rig, it is possible to survey the fatigue initiation and growth of material within a limited period of time.

Although the fatigue life is estimated to be within a few hours of rig's operation, there are some limitations inherent to the methodology of life prediction in this research. Among various factors the hardening, yield limit and wear in rail material can have influential effects on fatigue lives. The influence of such factors can be studied with the real experiments using the new test rig.

VII. CONCLUSION

A new test rig is developed for conducting RCF tests in rail material. In this paper, fatigue analysis was carried out using the numerical model of the test rig on the basis of finite element modelling and fatigue crack prediction technique. The results of fatigue life predictions were compared with the cyclic mechanism of the test rig to estimate the operational time of the experiments toward the crack initiation limit. The following conclusions can be drawn from the numerical simulations and comparisons:

1) The fatigue life of rail material in the test rig model was relatively close to the actual railway by applying the equivalent loading conditions in both models. More precisely, the fatigue life of material in the test rig model was around 9% smaller than that of the actual railway.
2) The ratchetting life of rail material in the test rig model was about 12% lower than the relative value of the actual railway, employing the equivalent loading conditions.
3) The crack initiation life of rail material was dominantly governed by cyclic fatigue (N_f) rather than ratchtting failure (N_r). This was occurred both for the test rig model and for the actual railway model.
4) A strong relationship between the fatigue life and the loading conditions was observed. A significant reduction in fatigue life was found, when the vertical load is increased. Likewise, the fatigue life was dramatically reduced for the larger traction coefficients.
5) The crack initiation life of material was dominantly affected by the presence of the surface defects. The maximum fatigue life was recorded for the smooth rail. When the size of defect is increased, lower fatigue lives were observed.
6) The manifestation of fatigue crack initiation was achieved within a few hours of test rig operation (around 4 hours for the selected loading history and material properties).
7) By applying the artificial defects or by changing the loading conditions, it was possible to accelerate the fatigue initiation of material.
8) The test rig was able to operate for a limited period of time, covering the fatigue crack initiation limit and the crack growth life. This can simulate the fatigue initiation and fatigue development of rail material with an accelerated mechanism.

REFERENCES

[1] E.E. Magel, "Rolling Contact Fatigue: A Comprehensive Review", Report, DOT/FRA/ORD-11/24, *Federal Railroad Administration*, 2011.

[2] D.T. Eadie, D. Elvidge, K. Oldknow, R. Stock, P. Pointner, J. Kalousek, P. Klauser, "The effects of top of rail friction modifier on wear and rolling contact fatigue: Full-scale fail-wheel test rig evaluation, analysis and modelling," *Wear*, vol. 265 (2008) pp. 1222-1230.

[3] U. Olofsson, T. Telliskivi, "Wear, plastic deformation and friction of two rail steels—a full-scale test and a laboratory study", *Wear*, vol. 254 (2003) pp. 80-93.

[4] J.H. Beynon, J.E. Garnham, K.J. Sawley, "Rolling contact fatigue of three pearlitic rail steels", *Wear*, vol. 192 (1996) pp. 94-111.

[5] W.R. Tyfour, J.H. Beynon, A. Kapoor, "Deterioration of rolling contact fatigue life of pearlitic rail steel due to dry-wet rolling-sliding line contact", *Wear*, vol. 197 (1996) pp. 255-265.

[6] R.I. Carroll, J.H. Beynon, "Decarburisation and rolling contact fatigue of a rail steel", *Wear*, vol. 260 (2006) pp. 523-537.

[7] G. Donzella, A. Mazzu, C. Petrogalli, "Competition between wear and rolling contact fatigue at the wheel-rail interface: some experimental evidence on rail steel", *IMech. Part F, J Rai*, vol. 223 (2009) pp. 31-44.

[8] J. Seo, S. Kwon, H. Jun, D. Lee, Rolling contact fatigue of white etching layer on pearlite steel rail, *Key Eng Mat*, vol. 417-418 (2010) 309-312.

[9] S. Pal, C. Valente, W. Daniel, M. Farjoo, "Metallurgical and physical understanding of rail squat initiation and propagation", *Wear*, vol. 284 (2012) pp. 30-42.

[10] D. Scott, J. Blackwell, "NEL rolling contact tests—accelerated service simulation tests for lubricants and materials for rolling elements", Wear, vol. 17 (1971) pp. 323-333.

[11] O. Zwirlein, H. Schlicht, "Rolling contact fatigue mechanisms—accelerated testing versus field performance, *Rolling contact fatigue testing of bearing steels*", vol. 771 (1982) pp. 358-379.

[12] J.J. Hoo, "Rolling Contact Fatigue Testing of Bearing Steels: A Symposium", *ASTM International,* 1982.

[13] S. Ito, N. Tsushima, H. Muro, "Accelerated rolling contact fatigue test by a cylinder-to-ball rig", *Rolling Contact Fatigue Testing of Bearing Steels*, (1982) pp. 125-135.

[14] D. Glover, "A ball-rod rolling contact fatigue tester, Rolling Contact" *Fatigue Testing of Bearing Steels*, ASTM STP, 771 (1982) pp. 107-125.

[15] J. Ciruna, H. Szieleit, "The effect of hydrogen on the rolling contact fatigue life of AISI 52100 and 440C steel balls", *Wear*, vol. 24 (1973) 107-118.

[16] E.A. Gallardo-Hernandez, R. Lewis, R.S. Dwyer-Joyce, Temperature in a twin-disc wheel/rail contact simulation, *Tribology International*, vol. 39 (2006) pp. 1653-1663.

[17] E. Gallardo-Hernandez, R. Lewis, "Twin disc assessment of wheel/rail adhesion", *Wear*, vol. 265 (2008) pp. 1309-1316.

[18] M. Takikawa, Y. Iriya, "Laboratory simulations with twin-disc machine on head check", *Wear*, vol. 265 (2008) pp. 1300-1308.

[19] J.E. Garnham, C.L. Davis, "The role of deformed rail microstructure on rolling contact fatigue initiation", *Wear*, vol. 265 (2008) pp. 1363-1372.

[20] W.J. Wang, W. Zhong, J. Guo, Q.Y. Liu, "Investigation on rolling contact fatigue and wear properties of railway rail", *Advanced Tribology*, (2009) pp. 327-328.

[21] W. Zhong, J.J. Hu, P. Shen, C.Y. Wang, Q.Y. Lius, "Experimental investigation between rolling contact fatigue and wear of high-speed and heavy-haul railway and selection of rail material", *Wear*, vol. 271 (2011) pp. 2485-2493.

[22] E. Kabo, A. Ekberg, P. Torstensson, T. Vernersson, "Rolling contact fatigue prediction for rails and comparisons with test rig results", *Proc. IMech., Part F: J Rail and Rapid Transit*, vol. 224 (2010) pp. 303-317.

[23] J.W. Ringsberg, "Life prediction of rolling contact fatigue crack initiation", *International J fatigue*, vol. 23 (2001) pp. 575-586.

[24] K. Johnson, "The strength of surfaces in rolling contact", *Proc. IMech., Part C: J Mechanical Engineering Science*, vol. 203 (1989) pp. 151-163.

[25] J. Ringsberg, M. Loo-Morrey, B. Josefson, A. Kapoor, J.H. Beynon, "Prediction of fatigue crack initiation for rolling contact fatigue", *International J Fatigue*, vol. 22 (2000) pp. 205-215.

[26] U. Zerbst, R. Lundén, K.O. Edel, R.A. Smith, "Introduction to the damage tolerance behaviour of railway rails – a review", *Engineering Fracture Mechanics*, vol. 76 (2009) pp. 2563-2601.

[27] B.R. You, S.B. Lee, A critical review on multiaxial fatigue assessments of metals, *International J Fatigue*, vol. 18 (1996) pp. 235-244.

[28] J. Das, S. Sivakumar, "An evaluation of multiaxial fatigue life assessment methods for engineering components", *International J Pressure Vessels and Piping*, vol. 76 (1999) pp. 741-746.

[29] J. Ringsberg, B. Josefson, "Finite element analyses of rolling contact fatigue crack initiation in railheads", *Proc. IMech., Part F: J Rail and Rapid Transit*, vol. 215 (2001) pp. 243-259.

[30] A. Ekberg, E. Kabo, "Fatigue of railway wheels and rails under rolling contact and thermal loading—an overview", *Wear*, vol. 258 (2005) pp. 1288-1300.

[31] Y. Jiang, H. Sehitoglu, "A model for rolling contact failure", *Wear*, vol. 224 (1999) pp. 38-49.

[32] Y. Jiang, "A fatigue criterion for general multiaxial loading, Fatigue and fracture of engineering materials and structures", 23 (2000) pp. 19-32.

[33] A. Kapoor, "A re-evaluation of the life to rupture of ductile metals by cyclic plastic strain", *Fatigue & fracture of engineering materials & structures*, vol. 17 (1994) pp. 201-219.

[34] J. Bannantine, "Fundamentals of metal fatigue analysis", *Prentice Hall*, 1990, (1990) 273.

[35] K. Smith, T. Topper, P. Watson, "A stress-strain function for the fatigue of metals (Stress-strain function for metal fatigue including mean stress effect)", J materials, vol. 5 (1970) pp. 767-778.

[36] D. Socie, "Multiaxial fatigue damage models", *J Engineering Materials and Technology*, vol. 109 (1987) pp. 293-298.

[37] J. Ringsberg, "Rolling contact fatigue of railway rails with emphasis on crack initiation", *Chalmers University of Technology*, 2000.

[38] A. Jaschinski, H. Chollet, S. Iwnicki, A. Wickens, J. Würzen, "The application of roller rigs to railway vehicle dynamics", *Vehicle System Dynamics*, vol. 31 (1999) pp. 345-392.

[39] T. Armstrong, D. Thompson, "Use of a reduced scale model for the study of wheel/rail interaction", *Proc. IMech., Part F: J Rail and Rapid Transit*, vol. 220 (2006) pp. 235-246.

[40] X. Zhao, Z. Li, "The solution of frictional wheel–rail rolling contact with a 3D transient finite element model: Validation and error analysis", *Wear*, vol. 271 (2011) pp. 444-452.

[41] J. Hallquist, "LS-DYNA Theoretical Manual", in, Livermore Software Technology Corporation: Livermore, California, 1998.

[42] J.-L. Chaboche, "Constitutive equations for cyclic plasticity and cyclic viscoplasticity", *International J Plasticity*, vol. 5 (1989) pp. 247-302.

[43] J. Lemaitre, J.-L. Chaboche, Mechanics of solid materials, *Cambridge University Press*, 1990.

[44] J.W. Ringsberg, "Cyclic ratchetting and failure of a pearlitic rail steel", *Fatigue & Fracture of Engineering Materials & Structures*, vol. 23 (2000) 747-758.

[45] M. Akama, H. Matsuda, H. Doi, M. Tsujie, "Fatigue crack initiation life prediction of rails using theory of critical distance and critical plane approach", *J Comp. Science and Technology*, vol. 6 (2012) pp. 54-69.

[46] X. Zhao, Z. Li, J. Liu, "Wheel–rail impact and the dynamic forces at discrete supports of rails in the presence of singular rail surface defects", *Proc. IMech., Part F: J Rail and Rapid Transit*, 226 (2012) pp. 124-139.

[47] Z. Li, X. Zhao, C. Esveld, R. Dollevoet, M. Molodova, "An investigation into the causes of squats—correlation analysis and numerical modeling", *Wear*, vol. 265 (2008) pp. 1349-1355.

[48] Z. Li, R. Dollevoet, M. Molodova, X. Zhao, "Squat growth—Some observations and the validation of numerical predictions", *Wear*, vol. 271 (2011) pp. 148-157.